Control of Tissue Homeostasis, Tumorigenesis, and

Degeneration by Coupled Bidirectional Bistable Switches

by

Diego Barra Avila

A Thesis Presented in Partial Fulfillment
of the Requirements for the Degree
Master of Science

Approved April 2021 by the
Graduate Supervisory Committee:

Xiaojun Tian, Chair
Xiao Wang
Christopher Plaisier

ARIZONA STATE UNIVERSITY

May 2021

ABSTRACT

The Hippo-YAP/TAZ signaling pathway plays a critical role in tissue homeostasis, tumorigenesis, and degeneration disorders. The regulation of YAP/TAZ levels is controlled by a complex regulatory network, where several feedback loops have been identified. However, it remains elusive how these feedback loops contain the YAP/TAZ levels and maintain the system in a healthy physiological state or trap the system into pathological conditions. Here, a mathematical model was developed to represent the YAP/TAZ regulatory network. Through theoretical analyses, three distinct states that designate the three physiological and pathological outcomes were found. The transition from the physiological state to the two pathological states is mechanistically controlled by coupled bidirectional bistable switches, which are robust to parametric variation and stochastic fluctuations at the molecular level. This work provides a mechanistic understanding of the regulation and dysregulation of YAP/TAZ levels in tissue state transitions.

TABLE OF CONTENTS

LIST OF TABLES

LIST OF FIGURES

CHAPTER 1

INTRODUCTION

The Hippo signaling pathway is responsible for organ size control, tissue homeostasis, and regeneration [1-3]. Dysfunction of this pathway has been associated with tumorigenesis and degenerative diseases [1, 4-6]. This pathway consists of several kinases that target two transcriptional coactivators, Yes-associated protein 1 (YAP) and WWRT PDZ binding motif (TAZ) [1-6]. Following the activation of the Hippo pathway, a phosphorylation cascade starting with NF2 leads to sequential activation of MST1/2 and LATS1/2, which further phosphorylates YAP/TAZ at specific serine residues, leading to the sequestration of YAP/TAZ in the cytoplasm for degradation via the ubiquitin-proteasome pathway [1-6]. When Hippo is inactivated, YAP/TAZ remains unphosphorylated and enters the nucleus, where it binds to several cofactors, such as TEAD, RUNX, or SMAD, and regulates gene expression of many targets [1-6]. Some of these targets also regulate the levels of YAP/TAZ and thus forms a complex regulatory network with many feedback loops. However, the roles of these feedback loops remain underexplored.

Homeostasis was proposed to be maintained through a negative feedback loop between YAP/TAZ and LATS1/2, where YAP/TAZ promotes LATS1/2 expression through TEAD/NF2 while LATS1/2 inactivates YAP/TAZ [7]. Dysfunction of Hippo signaling could lead to unregulated YAP/TAZ activity and thus increased cell proliferation, leading to tumorigenesis [1, 4]. But lack of YAP/TAZ activity and expression of its target genes has been observed to cause developmental defects and tissue degeneration [1, 5, 6]. Thus, proper regulation of the Hippo signaling pathway

allows for tissue to exist in a homeostatic state, but improper regulation can trap tissue in diseased states, either degenerative or tumorigenic.

Crosstalk between the Hippo-YAP/TAZ and Notch signaling pathway has been observed in several cancers. Notch ligand Jag1 was dependent on YAP/TAZ activity, and Notch intracellular domain (NICD) reduced TAZ degradation, thus placing YAP/TAZ and Notch signaling in a positive feedback loop in hepatocellular carcinoma (HCC) [8]. More evidence of this positive feedback loop can be found in rhabdomyosarcomas, as the core Notch transcription RPBJ regulated YAP1 through direct transcription, and NICD overexpression increased YAP1 levels [9]. Another positive feedback loop between YAP/TAZ and SIRT1 is associated with different types of tissue degeneration, such as neurodegeneration and retinal degeneration [1, 5, 6, 10, 11]. SIRT1 can deacetylate YAP and decrease its activity [10], while YAP can promote SIRT1 expression through Myc [10, 12, 13]. Thus, the YAP/TAZ level is regulated by several coupled feedback loops. However, it remains elusive how these feedback loops are orchestrated to control the YAP/TAZ level and thus the transition from tissue homeostasis to tumorigenesis or degenerative diseases.

In this work, we developed a mathematical model to recapitulate the YAP/TAZ regulatory network. Through theoretical analyses, we found three states with distinct levels of YAP/TAZ that designate tissue homeostasis, tumorigenesis, and degeneration, respectively. Coupled bidirectional bistable switches (CBBS) were found to control the transition from the homeostatic state to the tumorigenic or degenerative states. The homeostatic state is controlled by the YAP/TAZ/LATS negative feedback loop,

and the bidirectional bistable switches are governed by coupled positive feedback loops.

In addition, these conclusions are robust to parametric variation and molecular-level

fluctuations.

CHAPTER 2

MATERIALS AND METHODS

NETWORK CONSTRUCTION

To understand the regulation of YAP/TAZ activity and levels and its roles in tissue homeostasis, tumorigenesis, and degeneration, we built one mathematical model based on the regulatory network, as shown in Fig. 1. The Hippo signaling pathway regulates YAP/TAZ activity through phosphorylation. Upon Hippo signaling activation, LATS1/2 is activated to phosphorylate YAP/TAZ [1-6]. Dephosphorylation of YAP/TAZ is regulated by GPCR signaling [7]. In unphosphorylated form, YAP/TAZ stays in the nucleus and induces transcription of LATS2 [1], forming a negative feedback loop (Fig.1A, red lines). The interactions between unphosphorylated YAP/TAZ and SIRT1 form one positive feedback loop (Fig.1A, blue lines), in which SIRT1 promotes the transcription of YAP, while YAP promotes transcription of SIRT1 [10, 12, 13]. YAP/TAZ and Notch form another positive feedback loop (Fig.1A, green line), in which YAP/TAZ activates Notch signaling by transcribing for Notch ligands and promotes transcription of YAP [8, 9]. Table 1 in Appendix A summarizes the experimental evidence of this regulatory network. We used the following ordinary differential equations (ODEs) to describe the deterministic behavior of this regulatory network.

$$\frac{d[L]}{dt} = k_{L1} + k_{L2} \cdot \frac{[YT_{up}]^n}{[YT_{up}]^n + J_L^n} - k_{L3} \cdot [L] \tag{1}$$

$$\frac{d[YT_{up}]}{dt} = k_{YTup0} + k_{YTup1} \cdot \frac{[S]^n}{[S]^n + J_{YTup1}^n} + k_{YTup2} \cdot \frac{[N]^n}{[N]^n + J_{YTup2}^n} \tag{2}$$

$$+ k_{YTup3} \cdot \frac{[YT_{up}] \cdot [L]}{[YT_{up}] + J_{YTup3}} + k_{YTup4} \cdot \frac{[YT_p]}{[YT_p] + J_{YTup4}}$$

$$- k_{YTup5} \cdot [YT_{up}]$$

$$\frac{d[YT_p]}{dt} = k_{YTup3} \cdot \frac{[YT_{up}] \cdot [L]}{[YT_{up}] + J_{YTup3}} - k_{YTup4} \cdot \frac{[YT_p]}{[YT_p] + J_{YTup4}} - k_{YTp1} \cdot [YTp] \tag{3}$$

$$\frac{d[S]}{dt} = k_{S1} + k_{S2} \cdot \frac{[YT_{up}]^n}{[YT_{up}]^n + J_S^n} - k_{S3} \cdot [S] \tag{4}$$

$$\frac{d[N]}{dt} = k_{N1} + k_{N2} \cdot \frac{[YT_{up}]^n}{[YT_{up}]^n + J_N^n} - k_{N3} \cdot [N] \tag{5}$$

in which [L], [YT$_{up}$], [YT$_p$], [S], and [N] denote the concentrations of endogenous

LATS1/2, unphosphorylated YAP/TAZ, phosphorylated YAP/TAZ, SIRT1, and

NOTCH, respectively. For the phosphorylation reaction of YAP/TAZ by LATS1/2,

Michaelis-Menten kinetics were used. The function $\frac{[YT_{up}]*[L]}{[YT_{up}]+J_{YTup3}}$ represents the

phosphorylation of YAP/TAZ by LATS1/2. The function $\frac{[YT_p]}{[YT_p]+J_{YTup4}}$ was used to

represent the dephosphorylation of YAP/TAZ. Hill functions $\frac{J_{X_i}^n}{[X_i]+J_{X_i}^n}$ and $\frac{[X_i]^n}{[X_i]^n+J_{X_i}^n}$ were

used for all the transcription regulation in the network. In addition, the basal production

rate was assumed as constant, and the degradation rate was assumed proportional to the

protein concentration. Table 2 and Table 3 in Appendix A list the definition and the

initial value of each variable and a set of standard parameter values, respectively. The

default state is the tissue homeostatic state, in which the concentration of each species is

set to its stable steady state value in the standard parameter set.

5
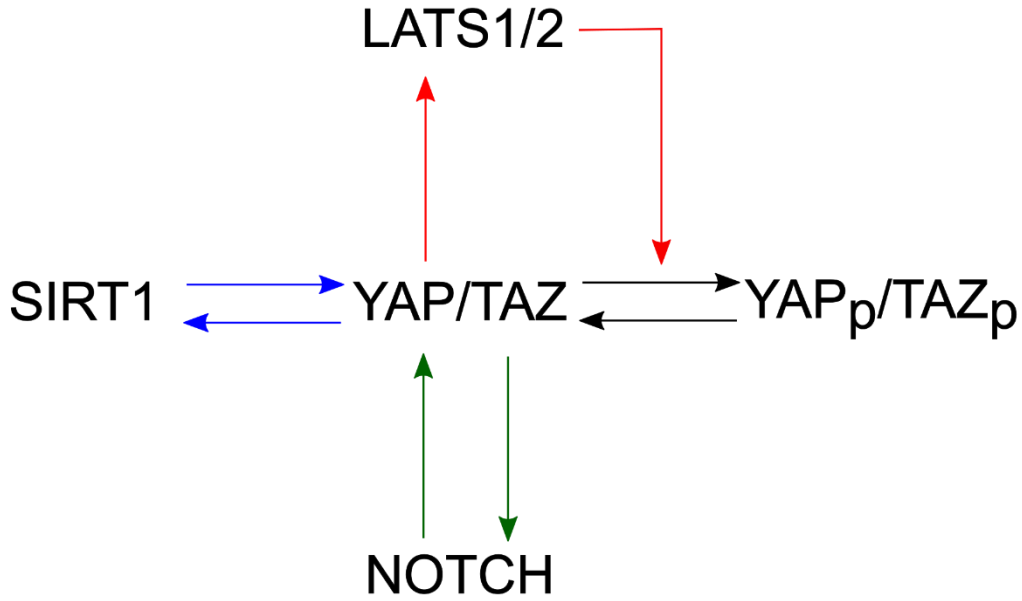
Figure 1: Schematic Depiction of the Regulatory Network of YAP/TAZ. LATS1/2 promotes the phosphorylation of YAP/TAZ [1-6], while YAP/TAZ promotes the transcription of LATS2, leading to cytoplasmic accumulation and subsequent degradation of YAP/TAZ [7]. YAP/TAZ promotes the Notch signaling pathway by inducing transcription of JAG1, DLL1, and RBPJ [8,9], while Notch signaling pathway promotes YAP/TAZ expression through RBPJ-binding to YAP1 promoter [8,9]. SIRT1 promotes YAP through Pol II-dependent transcription [12], while YAP/TAZ promotes SIRT1 transcription by upregulating MYC [13, 14].

To perform nullcline analysis, we simplified the above mathematical model into the following two-dimensional system,

$$\frac{d[L]}{dt} = k_{L1} + k_{L2} \cdot \frac{[YT_{up}]^n}{[YT_{up}]^n + J_L^n} - k_{L3} \cdot [L] \tag{6}$$

$$\frac{d[YT_{up}]}{dt} = k_{YTup0} + k_{YTup1} \cdot \frac{[S^*]^n}{[S^*]^n + J_{YTup1}^n} + k_{YTup2} \cdot \frac{[N^*]^n}{[N^*]^n + J_{YTup2}^n} \tag{7}$$

$$+ k_{YTup3} \cdot \frac{[YT_{up}] \cdot [L]}{[YT_{up}] + J_{YTup3}} + k_{YTup4} \cdot \frac{[YT_p^*]}{[YT_p^*] + J_{YTup4}}$$

$$- k_{YTup5} \cdot [YT_{up}]$$

The [L]-nullcline and [YT$_{up}$]-nullcline are determined by solving d[L]/dt = 0 and

d[YT$_{up}$]/dt = 0, respectively.

CHAPTER 3

RESULTS

TISSUE HOMEOSTASIS IS REGULATED BY YAP/TAZ/LATS NEGATIVE FEEDBACK LOOP

The Hippo signaling pathway regulates tissue homeostasis by using the YAP/TAZ-LATS1/2 negative feedback loop. We performed nullcline analysis to study how this negative feedback loop maintains tissue homeostasis. As shown in Fig. 2, the system only has one stable steady state at the intersection between the $[YT_{up}]$ and $[L]$ nullclines under the standard parameter set. This steady state corresponds to the homeostatic state. Plotting the time course of $[YT_{up}]$ using the reduced 2-ODE model, we see that for all various initial conditions, the system moves to the steady state. Trajectories with initial $[YT_{up}]$ values higher than that of the value of $[YT_{up}]$ at the steady state initially increase, but then decrease as the $[L]$ steady state is reached. The vector field and trajectories in Fig. 2A show that the $[L]$ steady state is reached before the $[YT_{up}]$ steady state is. Fig. 2B shows YAP/TAZ reaching its steady state after some time has passed. This time delay before YAP/TAZ is repressed by LATS1/2 towards its steady state can allow enough duration for YAP/TAZ to act as transcriptional coactivators [7]. This analysis allows us to see how the negative feedback loop between YAP/TAZ and LATS1/2 operates to maintain tissue homeostasis.
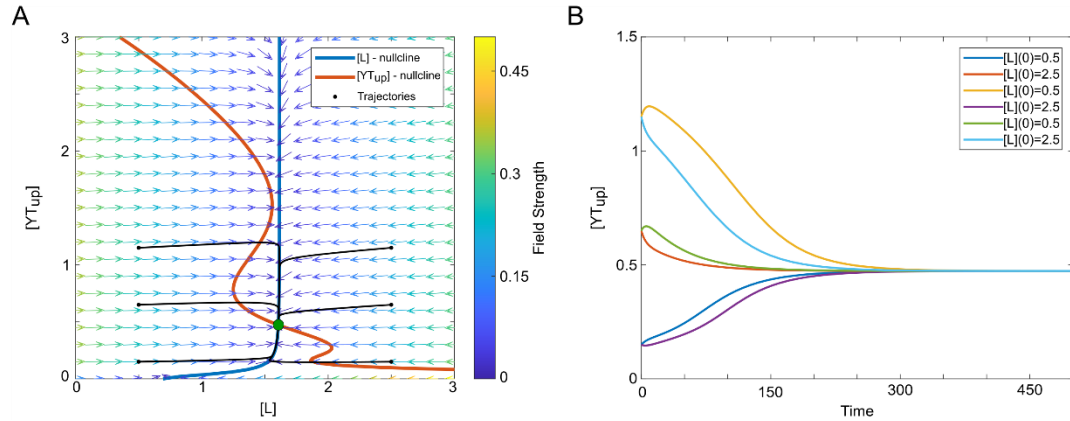
Figure 2: Tissue Homeostasis is Regulated by YAP/TAZ/LATS Negative Feedback Loop. (A) Nullcline analysis of the regulatory system shows one stable steady state (tissue homeostasis, green circle) at the intersections of the nullclines under the standard parameter set. The [L]-nullcline is drawn in blue and the [YT$_{up}$]-nullcline is drawn in red. The vector field of the system is represented by small arrows, where the color is proportional to the field strength. Example trajectories starting from different initial states were shown to represent the dynamics of the system towards the tissue homeostatic state. (B) The time course of the [YT$_{up}$] level with the system starting from a range of initial conditions.

THE TRANSITION TO TUMORIGENESIS OR DEGENERATION DISEASE IS REGULATED BY TWO COUPLED BI-DIRECTIONAL BISTABLE SWITCHES

To further understand how the YAP/TAZ levels are controlled by the regulatory network and how tissue states are determined by YAP/TAZ dynamics, we performed one-parameter bifurcation analysis over the basal production of YAP/TAZ k_{YTup0}. Here we used k_{YTup0} as the bifurcation parameter to represent any mutation or dysregulation in the system that could change the production rate of YAP/TAZ and thus change the tissue state. As shown in Fig. 3A, the dependence of the steady states of unphosphorylated YAP/TAZ on k_{YTup0} shows three different types of stable steady states. The middle branch (green line) with medium levels of YAP/TAZ corresponds to the tissue homeostatic state, while the bottom branch (blue line) with low levels of YAP/TAZ and the upper branch (red lines) with high levels of YAP/TAZ corresponds to the

8

degenerative and tumorigenic tissue states, respectively. This is consistent with the findings that reduced levels of YAP/TAZ were found in degenerative diseases and increased levels of YAP/TAZ were found in tumorigenic models [1, 5-9, 13, 15, 16].

The bifurcation diagram shows that two coupled bi-directional bistable switches are responsible for transitions among these tissue states. It noted that the system is monostable in the homeostatic state with a small variation of k_{YTup0} (green shaded region). However, as the value of k_{YTup0} reaches the saddle-node bifurcation point (SN1), the system transitions from the homeostatic state to the degenerative state (Fig. 3A, grey dashed lines with yellow arrows), which is controlled by the first bistable switch. The system can be recovered back only if k_{YTup0} reaches another threshold SN2, which is higher than SN1. That is, the system is monostable and immersed in the degenerative state when $k_{YTup0} <$ SN2 (blue shaded region) but shows bistability when SN1 $< k_{YTup0} <$ SN2 (cyan shaded region). The bistability in this region is also observed in the nullcline analysis (Fig. 3B). It is noted that the [L]-nullcline is the same as the one in Fig.2A, given that it is unaffected by the k_{YTup0} value. The $[YT_{up}]$-nullcline shifts to the left as k_{YTup0} decreases, and thus intersect with the [L]-nullcline at three steady states, two of which are stable steady states, corresponding to the homeostatic state (Fig. 3B, green circle) and the degenerative state (Fig. 3B, blue circle).

The second switch triggers the transition from the homeostatic state to the tumorigenic state (Fig. 3A, grey dashed lines with yellow arrows), as k_{YTup0} reaches the saddle-node bifurcation point (SN3). The system can be recovered back only if k_{YTup0} reaches another threshold SN2, which is higher than SN4. The system is trapped in the tumorigenic state when $k_{YTup0} >$ SN3 (red shaded region) and shows bistability when SN4

9

< k_{YTup0} < SN3 (yellow shaded region). In the phase plane (Fig. 3C), the [YT_{up}]-nullcline

shifts to the right as a result of k_{YTup0} and thus intersects with the [L]-nullcline with three

steady states, two of which are stable and correspond to the homeostatic state (Fig. 3C,

green circle) and the tumorigenic state (Fig. 3C, green circle). That is, this bistable switch

can ramp down to the degenerative state or switch up to the tumorigenic state, showing a

bidirectional nature. Thus, the transition from tissue homeostasis to tumorigenesis or

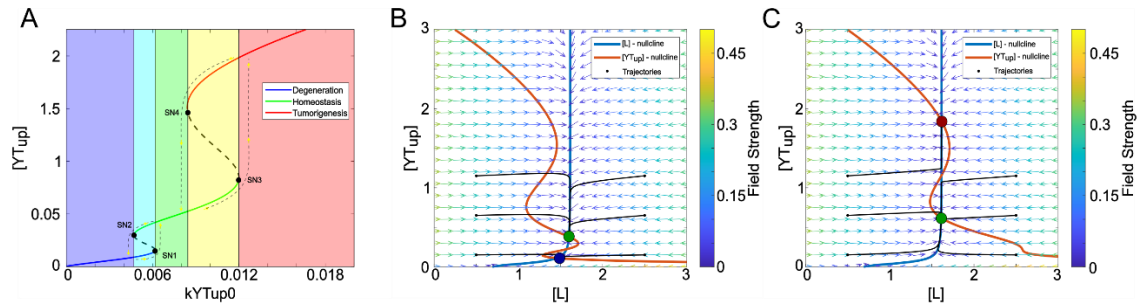degeneration disease is regulated by two coupled bi-directional bistable switches.

Figure 3: Bifurcation and Nullcline Analysis Display Three States. (A) The
bifurcation diagram shows the steady state of active/unphosphorylated YAP/TAZ as a
function of basal expression of unphosphorylated YAP/TAZ (k_{YTup0}). The labeled points
SN1, SN2, SN3, and SN4 indicate saddle-node bifurcation points. The lower blue branch,
middle green branch, and upper red branch are defined as the degenerative state,
homeostatic state, and tumorigenic state. The green shaded region shows the monostable
range within the homeostatic state, the blue shaded region shows the monostable range
within the degenerative state, and the red shaded region shows the monostable range
within the tumorigenic state. The cyan shaded region shows a bistable region with
degenerative and homeostatic states, while the yellow shaded region shows the bistable
region within the homeostatic and tumorigenic states. (B) Nullcline analysis of the
regulatory system shows the two stable steady states and one unstable steady state when
k_{YTup0} is within the first bistable region (between SN1 and SN2). Example trajectories
starting from different initial states were shown to represent the dynamics of the system
towards the tissue homeostatic and degenerative states. (C) Nullcline analysis of the
regulatory system shows the two stable steady states and one unstable steady state when
k_{YTup0} is within the second bistable region (between SN3 and SN4). Example trajectories
starting from different initial states were shown to represent the dynamics of the system
towards the tissue homeostatic and tumorigenic states.

EFFECT OF YAP/TAZ-LATS1/2 NEGATIVE FEEDBACK STRENGTH ON HOMEOSTASIS

Since we have understood the transitions among three outcomes in terms of the bi-directional bistable switches, here we explore the effect of the YAP/TAZ-LATS1/2 negative feedback strength on the range of monostability and the bistability in the bifurcation diagram. We perturbed the strength of this negative feedback by varying one parameter k_{YTup3}, the phosphorylation rate of YAP/TAZ by LATS1/2, from 85% to 115% of its original value, and studied how the bifurcation diagram changes. We found that by increasing the negative feedback strength k_{YTup3}, the range of the homeostatic state increases (Fig. 4A). This range is determined by the threshold SN2 and SN3. The dependence of SN2 and SN3 on the negative feedback strength k_{YTup3} is shown in the two-parameter diagram (Fig. 4B). We can see that both SN2 and SN3 increase with $k_{YTup3,}$ but SN3 increases faster, thus leading to the increased range of homeostatic state.

It is noted that the increase of SN3 with k_{YTup3} makes the transition from homeostatic state to the tumorigenic state difficult, but SN2 is increased as well at the time, which makes the transition from the homeostatic state to the degenerative state easier. Thus, the system faces a fundamental trade-off between these two pathological transitions, reducing the risk of tumorigenesis increases the risk of degeneration and vice versa. This result also suggests that targeting the YAP/TAZ-LATS1/2 negative feedback loop is not a good treatment design for degeneration diseases or cancer.

It is worth noting that when the negative feedback strength is small, the threshold SN4 could be smaller than SN1, which allows the coexistence of all three tissue states under the same condition. That is, the system shows tristability and the monostable range

11

of the homeostatic state vanished. In the two-parameter bifurcation diagram, the SN4

curve intersects with the SN1 curve at one point, which shows the transition from

tristability to the monostable homeostatic state (Fig. 4C). Under this condition, the

system may jump from the homeostatic state to either tumorigenesis or degenerative state

through large molecular variation. Fig. 4D shows the nullcline analysis when the system

exhibits tristability.

Thus, this is also not good and there is an optimal strength of the YAP/TAZ-

LATS1/2 negative feedback loop to make the monostable range of homeostatic state

large and both the risk of the transitions to tumorigenesis and degeneration small.
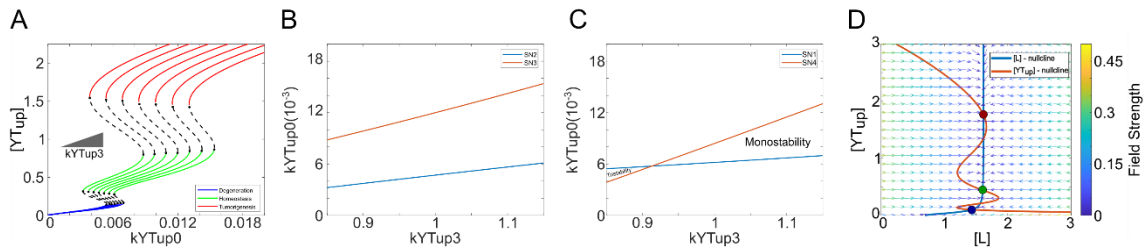
Figure 4: Effect of YAP/TAZ-LATS1/2 Feedback Strength on Homeostasis. (A) The parameter k_{YTup3}, characterizing the strength of the YAP/TAZ-LATS1/2 negative feedback loop, was varied from 85% to 115% (left to right), with 5% increments, of its original value to plot the 1-parameter bifurcation diagrams and show its effect on the homeostatic state. (B) 2-parameter bifurcation analysis was performed to observe how the thresholds SN2 and SN3 vary with k_{YTup3}. (C) 2-parameter bifurcation analysis was performed to observe how thresholds SN1 and SN4 vary with k_{YTup3}. The monostable range of the homeostatic state and the tristability range were both labeled to denote at which range of k_{YTup3} values they existed within. (D) Nullcline analysis of the regulatory system shows the three stable steady states and two unstable steady states when k_{YTup0} is within the tristable region (between SN1 and SN4) and k_{YTup3} is 85% of its original value.

BI-DIRECTIONAL BISTABLE SWITCHES IS ORCHESTRATED BY COUPLED

POSITIVE FEEDBACK LOOPS

To understand the design principle of the bi-directional bistable switches, we

performed a parameter sensitivity analysis for the transition thresholds (bifurcation points

SN1-4) by increasing and decreasing the value of each parameter by 15%. We found the

four bifurcations points to these parameter variations. That is, all three states exist with

these parameter variations. The fold changes of these thresholds were analyzed with each

parameter variation is in Fig. 5A-B. Thus, the bi-directional bistable switches display

robustness to these parameter variations.
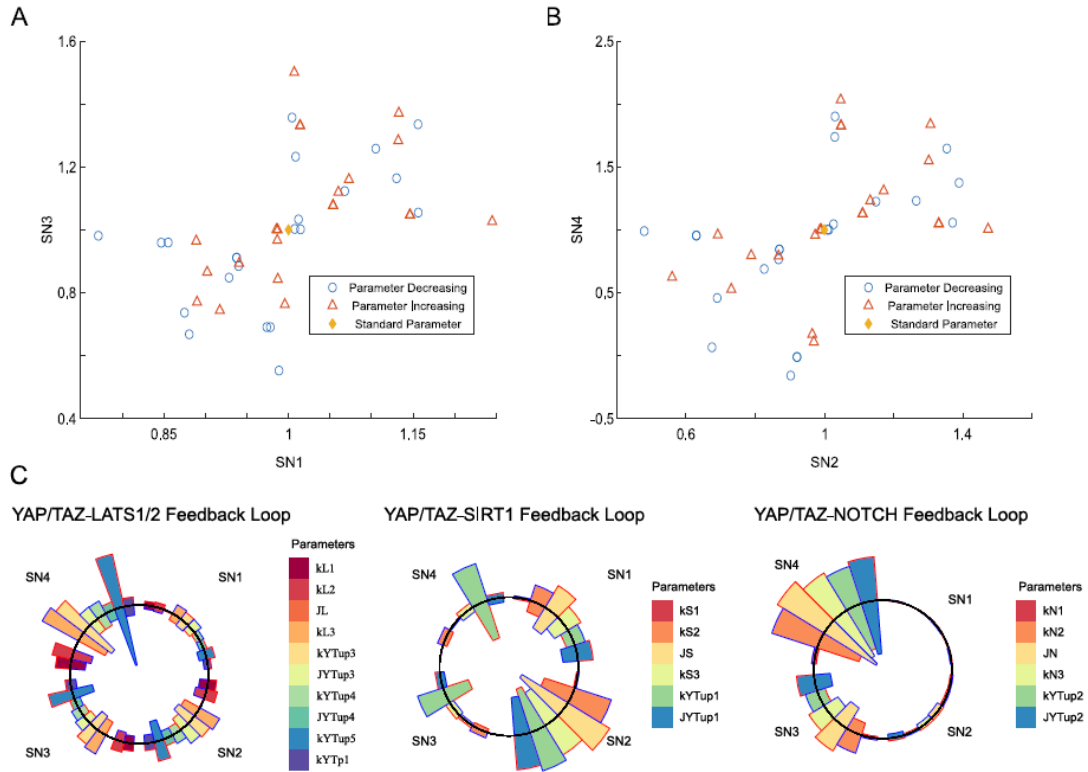
Figure 5: Bistable Switches Robust to Parameter Variation. (A) Parameter sensitivity analysis was performed for the transition thresholds SN1 and SN3 by individually increasing and decreasing each parameter by 15% and plotting the fold change. The diamond-shaped marker labeled as 'Standard Parameter' shows the initial start point of the thresholds. (B) Parameter sensitivity analysis was performed for the transition thresholds SN2 and SN4 by individually increasing and decreasing each parameter by 15% and plotting the fold change. The diamond-shaped marker labeled as 'Standard Parameter' shows the initial start point of the thresholds. (C) The circular bar plots show the percent changes in the thresholds when each of the parameters is increased and decreased by 15%. The red outline on the bars denote an increase of 15% in the parameter, while the blue outline denote a decrease of 15% in the parameter.

In addition, we determined which parameters both switches are more sensitive to. We found that the thresholds for the first switch (SN1 and SN2) are sensitive to the parameters in YAP/TAZ-SIRT1 positive feedback loop, while the thresholds for the second switch (SN3 and SN4) are sensitive to the parameters in the YAP/TAZ-NOTCH positive feedback loop. We found the thresholds for both switches to be sensitive to the parameters in the YAP/TAZ-LATS1/2 negative feedback loop, which comes to show the importance of this negative feedback loop in the regulation of the three states. This is consistent with Fig. 4. We do find an exception in which SN3 and SN4 are both sensitive to k_{YTup1}, a parameter within the YAP/TAZ-SIRT1 positive feedback loop. This exception can be due to how much more sensitive SIRT1 is to YAP/TAZ induction compared to NOTCH. Looking at the pseudo-steady state of SIRT1 and NOTCH, we observe that changes in YAP/TAZ affect SIRT1 much more than it does NOTCH. With the strength of induction of YAP/TAZ by SIRT1 already having a small value, any changes to it would affect the thresholds at which the system transitions between the physiological and pathological states.

To further demonstrate the dependence of thresholds for degeneration and tumorigenesis on the YAP/TAZ-SIRT1 and YAP/TAZ-NOTCH positive feedback loops, we performed 2-parameter bifurcation analysis. Fig. 6 shows the dependence of these thresholds on the feedback strengths of the two loops, the Michaelis constants of mutual activation between YAP/TAZ and SIRT1 (k_{YTup1} and k_{S2}) for the first loop, while the Michaelis constants of mutual activation between YAP/TAZ and NOTCH (k_{YTup2} and k_{N2}) for the second loop. We found that both thresholds decrease with increasing k_{YTup1} and k_{S2}, meaning induction of degeneration and tumorigenesis is regulated by the

14

YAP/TAZ-SIRT1 feedback loop. In comparison, only the threshold for activation of tumorigenesis is regulated by k_{YTup2} and k_{N2}, which is consistent with Fig.5.
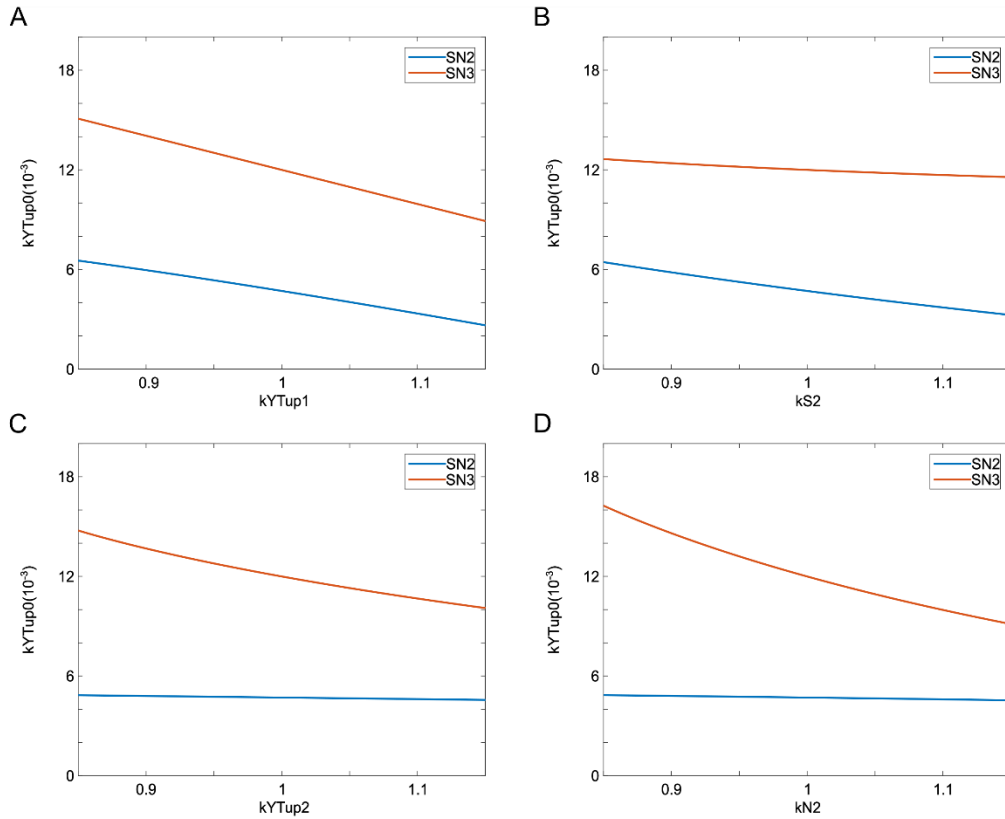
Figure 6: Dependence of Transition Thresholds by Feedback Loops' Strengths. 2 parameter bifurcation analyses show the dependence of normalized thresholds for activation of tissue degeneration and tumorigenesis based on the strength of (A-B) the YAP/TAZ SIRT1 feedback loop (k_{YTup1} and k_{S2}), and (C-D) YAP/TAZ-NOTCH feedback loop (k_{YTup2} and k_{N2}).

INFLUENCES OF NOISE ON THE TISSUE STATE TRANSITIONS

Extrinsic and intrinsic noises can affect the transitions between the defined states. Extrinsic noise can occur due to parameter variations to model cell-cell variability, while intrinsic noise is caused by low numbers of molecules per cell. To model these types of noise, we used a Tau-leap-based Gillespie algorithm to include intrinsic noise within the cell simulations, while the parameters within the system were varied by 5% to include extrinsic noise.

We used heatmaps to show cell counts with specific [N], [S], [YT$_{up}$] from the end of all cell simulations with only intrinsic noise when the k$_{YTup0}$ value was changed to 0.004, 0.005, 0.007, 0.012, and 0.014 from 0.0073, a value within the monostable region of the homeostatic state. In this analysis, the heatmap and distribution displaying simulation data when the standard value of k$_{YTup0}$ (0.007) was used to display the cells in the homeostatic state. We can observe the transition to the degenerative state when k$_{YTup0}$ values were set to 0.004 and 0.005, while the transition to the tumorigenic state can be observed when k$_{YTup0}$ values were set to 0.012 and 0.014 (Fig. 7A). The distribution of [YT$_{up}$] at the end of all cell simulations could better display the effect of adding extrinsic noise to the system, in addition to the present intrinsic noise. We plotted the [YT$_{up}$] distributions from 1000 cell simulations which included intrinsic and extrinsic noise, with 0% and 5% parameter variation (Fig. 7B). We observe the 5% parameter variation allows the appearance of cells in the tumorigenic state when the k$_{YTup0}$ value was changed to 0.004, while at the same time allowing more cells to exist in the homeostatic state even when k$_{YTup0}$ was changed to 0.014(Fig. 7B). Though most cells appear to be within the same state as when there was no parameter variation, the distribution of the cells within each state appears wider. It would be interesting to observe how changing the value of k$_{YTup0}$ back to its original value of 0.0073 would affect cells at the left-most side of the cell distribution seen in the degenerative state and those in the right-most side of the cell distribution seen in the tumorigenic state.

16
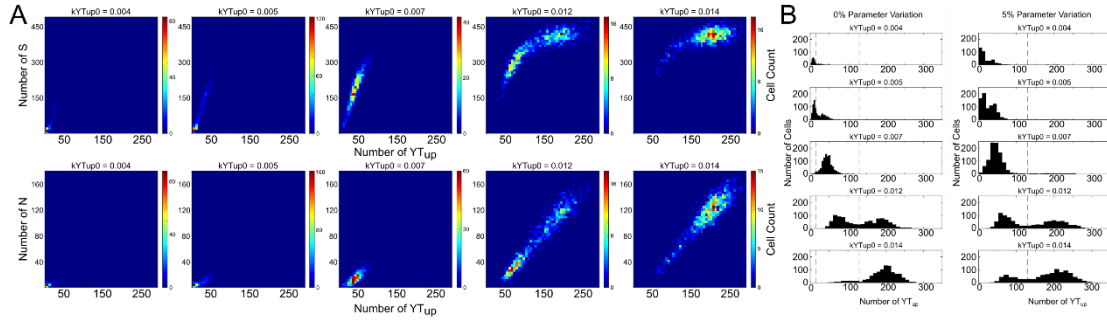
Figure 7: Effect of Intrinsic and Extrinsic Noise on Tissue State Transitions. (A) Concentration data from the end of 1000 cell simulations with intrinsic noise display the transition from the homeostatic state to the degenerative and tumorigenic states due to changes in the value of k_{YTup0}. The heatmaps with $k_{YTup0} = 0.007$ were used to display the cells in the homeostatic state. (B) The distributions of $[YT_{up}]$ from the end of 1000 cell simulations display the transition from the homeostatic state to the degenerative and tumorigenic states due to changes in the value of k_{YTup0} and different levels of extrinsic noise. The distribution with $k_{YTup0} = 0.007$ was used to display the cells in the homeostatic state.

CHAPTER 4

DISCUSSION

Tissue homeostasis requires a balance between cell proliferation and apoptosis. Disruption of this balance allows for the system to transition from a physiological state to a pathological one. Examining the role of Hippo signaling would provide an insight into how these transitions occur. The analysis performed on the regulatory network representing the Hippo signaling pathway showed how it regulates homeostasis, the transitions between physiological and pathological states, and the impact of noise on this network.

Regulatory networks with self-activation motifs have been observed to regulate state transitions through bistable switches, such as epithelial-to-mesenchymal transition. We found that the Hippo pathway also regulates the transition between physiological and pathological states with the use of coupled bidirectional bistable switches. Specifically, we found the YAP/TAZ-SIRT1 positive feedback loop to regulate the transition between the degenerative and homeostatic states, while the YAP/TAZ-NOTCH positive feedback loop regulated the transition between the homeostatic and tumorigenic state. In addition, the YAP/TAZ-LATS1/2 negative feedback loop was found to have a role in regulating both transitions, displaying its importance in maintaining tissue homeostasis.

Negative feedback loops are found in numerous biological systems to maintain homeostasis and robustness to perturbations. Here, the YAP/TAZ-LATS1/2 negative feedback loop strength was observed to have an impact on both the range of k_{YTup0} values on which homeostasis was possible as well as the range of monostability within this homeostatic region. We found that there was a tradeoff between making the monostable

region in the homeostatic state as large as possible and reducing the risk of the system

transitioning to a pathological state if we targeted the system through YAP/TAZ-

LATS1/2 feedback strength.

REFERENCES

1. Yu FX, Zhao B, Guan KL. Hippo pathway in organ size control, tissue homeostasis, and cancer. Cell. 2015;163(4):811-828.

2. Boopathy GT, Hong W. Role of hippo pathway-YAP/TAZ signaling in angiogenesis. Frontiers in cell and developmental biology. 2019;7:49.

3. Moya IM, Halder G. Hippo-YAP/TAZ signalling in organ regeneration and regenerative medicine. Nature reviews Molecular cell biology. 2019;20(4):211-226.

4. Park JH, Shin JE, Park HW. The role of hippo pathway in cancer stem cell biology. Molecules and cells. 2018;41(2):83.

5. Wang SP, Wang LH. Disease implication of hyper-Hippo signalling. Open biology. 2016;6(10):160119.

6. Sahu MR, Mondal AC. The emerging role of Hippo signaling in neurodegeneration. Journal of neuroscience research. 2020;98(5):796-814.

7. Moroishi T, Park HW, Qin B, Chen Q, Meng Z, Plouffe SW, et al. A YAP/TAZ-induced feedback mechanism regulates Hippo pathway homeostasis. Genes & development. 2015;29(12):1271-1284.

8. Kim W, Khan SK, Gvozdenovic-Jeremic J, Kim Y, Dahlman J, Kim H, et al. Hippo signaling interactions with Wnt/_-catenin and Notch signaling repress liver tumorigenesis. The Journal of clinical investigation. 2017;127(1):137-152.

9. Slemmons KK, Crose LE, Riedel S, Sushnitha M, Belyea B, Linardic CM. A novel notch-YAP circuit drives stemness and tumorigenesis in embryonal rhabdomyosarcoma. Molecular Cancer Research. 2017;15(12):1777-1791.

10. Yuan F, Wang J, Li R, Zhao X, Zhang Y, Liu B, et al. A new regulatory mechanism between P53 And YAP crosstalk By SIRT1 mediated deacetylation to regulate cell cycle and apoptosis in A549 cell lines. Cancer management and research. 2019;11:8619.

11. Tang BL, Chua CEL. SIRT1 and neuronal diseases. Molecular aspects of medicine. 2008;29(3):187-200.

12. Wang Y, Cui R, Zhang X, Qiao Y, Liu X, Chang Y, et al. SIRT1 increases YAP- and MKK3-dependent p38 phosphorylation in mouse liver and human hepatocellular carcinoma. Oncotarget. 2016;7(10):11284.

13. Choi W, Kim J, Park J, Lee DH, Hwang D, Kim JH, et al. YAP/TAZ initiates gastric tumorigenesis via upregulation of MYC. Cancer research. 2018;78(12):3306-3320.

14. Yuan F, Liu L, Lei Y, Tang P. p53 inhibits the upregulation of sirtuin 1 expression induced by c-Myc. Oncology letters. 2017;14(4):4396-4402.

15. Zhang C, Wang F, Xie Z, Chen L, Sinkemani A, Yu H, et al. Dysregulation of YAP by the Hippo pathway is involved in intervertebral disc degeneration, cell contact inhibition, and cell senescence. Oncotarget. 2018;9(2):2175.

16. Zhang C, Wang F, Xie Z, Chen L, Sinkemani A, Yu H, et al. AMOT 130 linking F-actin to YAP is involved in intervertebral disc degeneration. Cell proliferation. 2018;51(6):e12492.

17. Zheng Y, Liu C, Ni L, Liu Z, Mirando AJ, Lin J, et al. Cell type-specific effects of Notch signaling activation on intervertebral discs: Implications for intervertebral disc degeneration. Journal of cellular physiology. 2018;233(7):5431–5440.

18. Long J, Wang X, Du X, Pan H, Wang J, Li Z, et al. JAG2/Notch2 inhibits intervertebral disc degeneration by modulating cell proliferation, apoptosis, and extracellular matrix. Arthritis research & therapy. 2019;21(1):1–14.

19. Wang D, Hu Z, Hao J, He B, Gan Q, Zhong X, et al. SIRT1 inhibits apoptosis of degenerative human disc nucleus pulposus cells through activation of Akt pathway. Age. 2013;35(5):1741–1753.

20. Guo J, Shao M, Lu F, Jiang J, Xia X. Role of Sirt1 plays in nucleus pulposus cells and intervertebral disc degeneration. Spine. 2017;42(13):E757–E766.

APPENDIX A

COLLECTED DATA, PARAMETERS, AND DESCRIPTIONS FOR

MATHEMATICAL MODELS

Table 1: Summary of Experimental Support for Regulatory Network

Descriptions	References
Unphosphorylated YAP/TAZ promotes transcription of LATS1/2	[7]
LATS1/2 promotes phosphorylation of YAP/TAZ	[1-6]
Unphosphorylated YAP/TAZ promotes transcription of NOTCH	[8,9]
NOTCH promotes transcription of YAP/TAZ	[8, 9]
Unphosphorylated YAP/TAZ promotes transcription of SIRT1	[13, 14]
SIRT1 promotes transcription of YAP/TAZ	[12]

Table 2: Variables of Model

Variables	Description	Initial Values
$[YT_{up}]$	Concentration of unphosphorylated YAP/TAZ	0.4732
$[YT_p]$	Concentration of phosphorylated YAP/TAZ	0.2387
$[L]$	Concentration of LATS1/2	1.6057
$[S]$	Concentration of SIRT1	2.0886
$[N]$	Concentration of Notch signaling components and NICD	0.1697

Table 3: Parameters of Differential Equation System

Parameter	Description	Value
k_{L1}	Basal production rate of LATS1/2	0.15
k_{L2}	Production rate of LATS1/2	0.2
J_L	Michaelis constant of YAP/TAZ-dependent activation of LATS1/2 production	0.05
k_{L3}	Degradation rate of LATS1/2	0.2166
$k_{YT_{up}1}$	Production rate of YAP/TAZ induced by SIRT1	0.0225
$J_{YT_{up}1}$	Michaelis constant of SIRT1-dependent activation of YAP/TAZ production	1
$k_{YT_{up}2}$	Production rate of YAP/TAZ induced by NOTCH	0.105
$J_{YT_{up}2}$	Michaelis constant of NOTCH-dependent activation of YAP/TAZ production	1
$k_{YT_{up}3}$	Rate of YAP/TAZ phosphorylation by LATS1/2	0.045
$J_{YT_{up}3}$	Michaelis constant of LATS1/2-dependent activation of YAP/TAZ phosphorylation	1

$k_{YT_{up}4}$	Rate of YAP/TAZ dephosphorylation	0.05
$J_{YT_{up}4}$	Michaelis constant of protein-dependent activation of YAP/TAZ dephosphorylation	1
$k_{YT_{up}5}$	Degradation rate of unphosphorylated YAP/TAZ	0.033
$k_{YT_{p}1}$	Degradation rate of phosphorylated YAP/TAZ	0.05
k_{S1}	Basal production rate of SIRT1	0.01
k_{S2}	Production rate of SIRT1 induced by YAP/TAZ	1
J_S	Michaelis constant of YAP/TAZ-dependent activation of SIRT1 production	0.5
k_{S3}	Degradation rate of SIRT1	0.231
k_{N1}	Basal production rate of NOTCH	0.01
k_{N2}	Production rate of NOTCH induced by YAP/TAZ	0.525
J_N	Michaelis constant of YAP/TAZ-dependent activation of NOTCH	1.95
k_{N3}	Degradation rate of NOTCH	0.231
n	Hill coefficient	2

Table 4: Description of Differential Equation Terms

Term	Description
k_{L1}	Basal production of LATS1/2
$k_{L2} * \dfrac{[YT_{up}]^n}{[YT_{up}]^n + J_L{}^n}$	Production of LATS1/2 induced by YAP/TAZ
$k_{L3} * [L]$	Degradation of LATS1/2
$k_{YT_{up}0}$	Basal production of YAP/TAZ
$k_{YT_{up}1} * \dfrac{[S]^n}{[S]^n + J_{YT_{up}1}{}^n}$	Induction of YAP/TAZ production by SIRT1
$k_{YT_{up}2} * \dfrac{[N]^n}{[N]^n + J_{YT_{up}2}{}^n}$	Induction of YAP/TAZ production by NOTCH

$k_{YT_{up}3} * \dfrac{[YT_{up}] * [L]}{[YT_{up}] + J_{Y_{Tup}3}}$	Phosphorylation of YAP/TAZ by LATS1/2
$k_{YT_{up}4} * \dfrac{[YT_p]}{[YT_p] + J_{YT_{up}4}}$	Dephosphorylation of YAP/TAZ
$k_{YT_{up}5} * [YT_{up}]$	Degradation of unphosphorylated YAP/TAZ
$k_{Y_p1} * [YT_p]$	Degradation of phosphorylated YAP/TAZ
k_{S1}	Basal production of SIRT1
$k_{S2} * \dfrac{[YT_{up}]^n}{[YT_{up}]^n + J_S}$	Induction of SIRT1 production by YAP/TAZ
$k_{S3} * [S]$	Degradation of SIRT1
k_{N1}	Basal production of NOTCH
$k_{N2} * \dfrac{[YT_{up}]^n}{[YT_{up}]^n + J_N{}^n}$	Induction of NOTCH production by YAP/TAZ
$k_{N3} * [N]$	Degradation of NOTCH

Table 5: Stochastic Version of Model

Reaction	Description	Propensity function
$\emptyset \rightarrow L$	Basal production of LATS1/2	$k_{L1} * \Omega$
$\emptyset \rightarrow L$	Induction of LATS1/2 production	$k_{L2} * \dfrac{\left(\dfrac{YT_{up}}{\Omega}\right)^n}{\left(\dfrac{YT_{up}}{\Omega}\right)^n + J_L^n} * \Omega$
$L \rightarrow \emptyset$	Degradation of LATS1/2	$k_{L3} * L$
$\emptyset \rightarrow YT_{up}$	Basal production of YAP/TAZ	$k_{YT_{up}0}$
$\emptyset \rightarrow YT_{up}$	Induction of YAP/TAZ production by SIRT1	$k_{YT_{up}1} * \dfrac{\left(\dfrac{S}{\Omega}\right)^n}{\left(\dfrac{S}{\Omega}\right)^n + J_{YT_{up}1}^n} * \Omega$
$\emptyset \rightarrow YT_{up}$	Induction of YAP/TAZ production by NOTCH	$k_{YT_{up}2} * \dfrac{\left(\dfrac{N}{\Omega}\right)^n}{\left(\dfrac{N}{\Omega}\right)^n + J_{YT_{up}2}^n} * \Omega$

$YT_{up} \rightarrow YT_p$	Phosphorylation of YAP/TAZ by LATS1/2	$k_{YT_{up}3} * \dfrac{\dfrac{YT_{up} * L}{\Omega^2}}{\dfrac{YT_{up}}{\Omega} + J_{YT_{up}3}} * \Omega$
$YT_p \rightarrow YT_{up}$	Dephosphorylation of YAP/TAZ	$k_{YT_{up}4} * \dfrac{\dfrac{YT_p}{\Omega}}{\dfrac{YT_p}{\Omega} + J_{YT_{up}4}} * \Omega$
$YT_{up} \rightarrow \emptyset$	Degradation of unphosphorylated YAP/TAZ	$k_{YT_{up}5} * YT_{up}$
$YT_p \rightarrow \emptyset$	Degradation of phosphorylated YAP/TAZ	$k_{YT_p1} * YT_p$
$\emptyset \rightarrow S$	Basal production of SIRT1	$k_{S1} * \Omega$
$\emptyset \rightarrow S$	Induction of SIRT1 production by YAP/TAZ	$k_{S2} * \dfrac{\left(\dfrac{YT_{up}}{\Omega}\right)^n}{\left(\dfrac{YT_{up}}{\Omega}\right)^n + J_S^n} * \Omega$
$S \rightarrow \emptyset$	Degradation of SIRT1 production	$k_{S3} * S$
$\emptyset \rightarrow N$	Basal production of NOTCH	$k_{N1} * \Omega$
$\emptyset \rightarrow N$	Induction of NOTCH by YAP/TAZ	$k_{N2} * \dfrac{\left(\dfrac{YT_{up}}{\Omega}\right)^n}{\left(\dfrac{YT_{up}}{\Omega}\right)^n + J_N^n} * \Omega$
$N \rightarrow \emptyset$	Degradation of NOTCH	$k_{N3} * N$

Table 6: Evidence Linking Proteins to Disease States:

Protein	Degeneration	Tumorigenesis
YAP/TAZ	Downregulated [1, 5, 6, 15, 16]	Upregulated [1, 7-9, 12, 13]
LATS1/2	Downregulated [15, 16]	Upregulated [7]
NOTCH	Downregulated [17, 18]	Upregulated [8, 9]
SIRT1	Downregulated [11, 19, 20]	Upregulated [10, 12-14]